Analysis of two independent methods for retrieving liquid water profiles in spring and summer Arctic boundary clouds

U. Löhnert,[1] G. Feingold,[2] T. Uttal,[2] A. S. Frisch,[3] and M. D. Shupe[4]

Received 20 August 2002; revised 19 November 2002; accepted 9 January 2003; published 10 April 2003.

[1] A large number of all-liquid, nondrizzling stratus clouds (163 hours of measurements) were observed with a dual-channel microwave radiometer and a colocated 35-GHz cloud radar during the spring and summer months of the Surface Heat Budget of the Arctic Ocean (SHEBA) project. An algorithm developed by *Frisch et al.* [1995, 1998] to derive the liquid water content (LWC) is applied to these measurements assuming constant cloud drop number density and cloud drop size distribution breadth with height. A second algorithm developed by *Löhnert et al.* [2001] is specifically adapted for SHEBA clouds using a priori information from a large eddy simulation (LES) model initialized with summertime SHEBA radiosondes; about 50 soundings during nondrizzling, low-level, all-liquid water clouds are used. Using model-derived drop size distributions, a relationship between simulated radar reflectivity (Z) and model LWC is derived as well as an a priori LWC profile. Once the theoretical error covariance matrix of the Z-LWC relation is derived and the covariance matrix of the LWC profile is calculated, an optimal estimation method is applied to the SHEBA data. The Frisch et al. and Löhnert et al. methods are also applied to the LES model output, resulting in overall root-mean-square differences on the order of 30 to 60%. Both methods are sensitive to the assumed accuracies of the microwave-radiometer-derived LWP. When applied to LES model output, the Frisch et al. method shows a LWC overestimation in the lower parts of the cloud. These systematic errors are induced by the assumption of constant cloud number concentration with height. *INDEX TERMS:* 0320 Atmospheric Composition and Structure: Cloud physics and chemistry; 3307 Meteorology and Atmospheric Dynamics: Boundary layer processes; 3337 Meteorology and Atmospheric Dynamics: Numerical modeling and data assimilation; 3360 Meteorology and Atmospheric Dynamics: Remote sensing; 3394 Meteorology and Atmospheric Dynamics: Instruments and techniques; *KEYWORDS:* comparison of Arctic cloud liquid water profiles, sensor synergy, active and passive ground-based remote sensing, optimal estimation, LES model with explicit microphysics, cloud liquid water algorithms

Citation: Löhnert, U., G. Feingold, T. Uttal, A. S. Frisch, and M. D. Shupe, Analysis of two independent methods for retrieving liquid water profiles in spring and summer Arctic boundary clouds, *J. Geophys. Res.*, *108*(D7), 4219, doi:10.1029/2002JD002861, 2003.

1. Introduction

[2] A key towards understanding the impact of clouds on the Arctic climate system is quantifying macrophysical and microphysical cloud properties. On the one hand, clouds reflect incoming solar radiation directly back to space leading to a decreased availability of energy below the cloud and at the ground. On the other hand, clouds re-emit radiation in the thermal part of the energy spectrum and can thus enhance the greenhouse effect. Generally, cloud parameters, such as cloud phase, droplet size and water content, strongly influence the energy exchange between surface, cloud, atmosphere and space and thus impact heating rates at the surface and within the atmosphere. In terms of monitoring clouds, ground-based remote sensing measurements are by far the most sophisticated approach towards collecting long-term and temporally highly resolved cloud data.

[3] In 1997/1998 the Surface Heat Budget of the Arctic Ocean (SHEBA) project [*Uttal et al.*, 2002] collected a year's worth of continuous cloud observations at an ice camp, which drifted in the Arctic Ocean north of Alaska. Two cloud-monitoring instruments present at the SHEBA site were a 35-GHz cloud radar and a dual-channel microwave radiometer operating at 23.8 and 31.4 GHz. Cloud radars are able to remotely sense the vertical position of a cloud by measuring the radar reflectivity factor Z, which is the backscattered signal of a microwave radiation pulse originating from the radar transmitter. At 35 GHz scattering on nonprecipitating cloud drops occurs within the Rayleigh scattering regime [*Ulaby et al.*, 1981], which means that radar reflectivity is proportional to the sixth power of the cloud drop size radius. However, this dependency provides

[1]Meteorological Institute, University of Bonn, Bonn, Germany.
[2]Environmental Technology Laboratory, NOAA, Boulder, Colorado, USA.
[3]Cooperative Institute for Research in the Atmosphere, Boulder, Colorado, USA.
[4]Science and Technology Corporation, Boulder, Colorado, USA.

0148-0227/03/2002JD002861$09.00

only limited information on the cloud water content, which is proportional to the radius cubed.

[4] The complementary dual-channel microwave radiometer can give quite accurate information on the liquid water path (LWP), since it passively receives microwave radiation emitted by clouds and water vapor. Together, these instruments can be used to obtain liquid water content (LWC) profiles [*Frisch et al.*, 1995].

[5] This study focuses on the retrieval of LWC profiles during the spring and summer months of SHEBA. Several cases of all-liquid stratus cloud were observed during this time [*Curry et al.*, 2000; *Shupe et al.*, 2001]. These resulted from moist (relatively warm) air being advected over the cold ice. A common approach for determining LWC profiles from cloud radar and microwave radiometer is the algorithm proposed by *Frisch et al.* [1995, 1998], which is described in section 2.1. This approach assumes constant droplet number concentration and distribution breadth with height and is independent of systematic radar calibration errors. A second approach used in this study is the method according to *Löhnert et al.* [2001] (section 2.2), which has been used to retrieve LWC profiles of stratocumulus clouds over continental Europe. Here, this method is adapted to an Arctic environment using a priori information from large eddy simulation (LES) model runs. In section 3 we analyze the differences between both approaches by applying them to the all-liquid stratus data as classified by *Shupe et al.* [2001] from the SHEBA campaign. The methods are also assessed by applying them to LES model output, which can be considered as "truth" for this purpose. Finally, section 4 examines how the Frisch et al. algorithm is influenced by the microphysical assumptions of constant cloud drop number density (N) and constant droplet size distribution (DSD) breadth with height.

2. Theoretical Background

2.1. *Frisch et al.* [1995, 1998] Method

[6] This retrieval was derived for all-liquid, nondrizzling stratus clouds, applying certain constraints on cloud microphysics. *Frisch et al.* [1995] assume that cloud DSDs are adequately described by a lognormal function. The moments of the lognormal distribution can be calculated analytically, and consequently an expression for cloud liquid water content can be derived:

$$\mathrm{LWC} = (4\pi/3)\cdot\rho_w N r_0^3 \exp\left(9\sigma^2/2\right), \tag{1}$$

with σ defining the logarithmic distribution breadth (the geometric standard deviation), N the droplet number density, r_0 the distribution geometric mean radius and ρ_w the density of liquid water. The radar reflectivity factor (Z) can be determined as

$$Z = 2^6 N r_0^6 \exp\left(18\sigma^2\right). \tag{2}$$

An equation for LWC in terms of Z and LWP can only be derived in the following form if the assumption is made that N and σ are constant with height:

$$\mathrm{LWC}_h = \frac{\mathrm{LWP}}{\Delta z_h}\cdot\frac{\sqrt{Z_h}}{\sum_{j=1}^{M}\sqrt{Z_j}}, \tag{3}$$

with h denoting the specific height index, M the number of cloud levels and Δz the vertical extent of the radar reflectivity range gate. This equation implies that the vertical integral of LWC will always be exactly equal to the microwave-radiometer-derived LWP. *Frisch et al.* [1998] (hereinafter referred to as F98) showed that this retrieval is independent of radar calibration offsets and that equation (3) can be derived independently of the assumption of a lognormal DSD as long as the third moment of the DSD is linearly related to the sixth moment, a condition which drizzle free clouds may fulfil.

2.2. *Löhnert et al.* [2001] Method

[7] This method uses optimal estimation theory [e.g., *Rodgers*, 2000] to combine microwave-radiometer-derived LWP, radar reflectivity measurements, and a priori information about the LWC profile. Unlike the F98 method, the *Löhnert et al.* [2001] (hereinafter referred to as L01) method does not assume constant N and σ with height and a lognormal DSD, but rather certain statistical assumptions concerning the DSD, which are derived from a cloud model. A similar approach was taken by *McFarlane et al.* [2002], who used prior probability distributions of the 2nd, 3rd and 6th moments of the DSD measured by aircraft probes to infer optical depth, effective radius, and LWC of nonprecipitating clouds within a Bayesian algorithm.

[8] Within the L01 method the LWC profile is, to a certain degree, constrained to a functional relationship between Z and LWC

$$dBZ = a + b\cdot\log_{10}(\mathrm{LWC}), \tag{4}$$

with $dBZ = 10\log_{10}(Z/Z_0)$ ($\log_{10}$ hereinafter referred to as log), $Z_0 = 1\ \mathrm{mm^6\ m^{-3}}$ and a and b denoting least squares coefficients. The coefficients a and b are derived from an LES model described in the following subsection. This form of a Z-LWC relationship is frequently used to obtain LWC [*Fox and Illingworth*, 1997; *Liao and Sassen*, 1994]. However, applying it without any physical constraints can result in large errors [*Löhnert et al.*, 2001] due to the fact that Z is much more sensitive to larger drizzle drops than LWC. The LWC profile is also partly constrained to the microwave-radiometer-derived LWP:

$$\mathrm{LWP} = \sum_{j=1}^{M}\mathrm{LWC}_j\cdot\Delta z_j. \tag{5}$$

Together, equations (4) and (5) can be regarded as the forward model (F), which is inverted to obtain the LWC profile. The inversion procedure additionally uses an a priori profile of log(LWC) to stabilize the inversion. It is derived from the LES model as a mean profile over all nonprecipitating model profiles and can thus be regarded as an additional (simulated) measurement of log(LWC), but with an appropriate large error. The a priori profile will effectively smooth the solution and reduce the impact of such dBZ variations with height, which are not related to a significant change in log(LWC). Additionally, by taking into account the covariances of log(LWC) in height (equation (9)) the solution is constrained to a physically sensible form. This is due to the fact that by including the covariances of the model log(LWC) profiles, the retrieved

log(LWC) value in one height will depend on the values in all other heights and vice versa. Within the inversion procedure an optimal solution is found by maximizing the conditional probability density function of log(LWC) given *dBZ*, LWP, and the a priori profile following Bayesian theorem. For this procedure knowledge of the error in each measurement, as well as in F, is required. These determine to what degree the solution is constrained to each measurement, respectively the a priori profile. The assumed errors of *dBZ*, the *dBZ*-log(LWC) relationship, the microwave radiometer derived-LWP, and the a priori log(LWC) profile are described by an error covariance matrix, respectively a covariance matrix, all derived from the LES model. Following sections 2e and 4b of *Löhnert et al.* [2001], an iterative equation can be derived for the log(LWC) profile. In vector notation (bold face variables) we have

$$\log(\mathbf{LWC})_{i+1} = \log(\mathbf{LWC})_i + \left(\mathbf{S}_{ap}^{-1} + \mathbf{K}_i^T \mathbf{S}_\varepsilon^{-1} \mathbf{K}_i\right)^{-1} \times \left[\mathbf{K}_i^T \mathbf{S}_\varepsilon^{-1} \left(\mathbf{y} - \mathrm{F}\left(\log(\mathbf{LWC})_i\right)\right) - \mathbf{S}_{ap}^{-1} \left(\log(\mathbf{LWC})_i - \overline{\log(\mathbf{LWC})}\right)\right] \quad (6)$$

The variables of equation (6) are listed in Table 1. To apply equation (6), all variables and their errors must be Gaussian distributed. We use log(LWC) in equation (6) rather than LWC because log(LWC) more closely resembles a Gaussian distribution than LWC, since the latter exhibits many small LWC and few large LWC values.

2.2.1. LES Model

[9] In contrast to the method described by *Löhnert et al.* [2001], where a single column cloud model was used, we use the Regional Atmospheric Modelling System (RAMS) in a LES configuration. A previous study [*Jiang et al.*, 2001] demonstrated the capability of RAMS to simulate aerosol effects on the radiative properties of low-level stratus clouds during SHEBA. The model resolves the size distribution of cloud drops into 25 size bins. It is therefore ideally suited for calculation of *Z* and LWC and can also be used to derive the a priori profile of log(LWC) and the corresponding covariance matrix, as well as the relation between *dBZ* and log(LWC). To create representative model outputs, about 50 radiosonde profiles during conditions with low-level liquid water clouds as detected by cloud radar and microwave radiometer [*Shupe et al.*, 2001] are used to initialize the model.

[10] The current study uses the same model described by *Jiang et al.* [2001], except for the following. First, RAMS is run in a two-dimensional mode instead of a three-dimensional mode due to computing time constraints. Comparisons between two- and three-dimensional simulations for a single run show no significant statistical differences in the moments of the DSD. And second, the grid size is set to 45 m in the horizontal and 45 m in the vertical, in contrast to 25 m in the vertical used by *Jiang et al.* [2001], in order to match the vertical resolution of the cloud radar. Model simulation time is five hours with 2 s temporal resolution. However, model output is only stored at 5 min temporal resolution. Commonly, the initial model input parameters are physically unbalanced, which may lead to unrealistic values of the model output parameters at the beginning of each simulation (spin-up process). Due to this fact, the first hour of model output is not used. Since it is our goal to create statistically representative LWC profiles and not to reproduce the measurements in an exact way, the number of cloud condensation nuclei and the large-scale subsidence are randomly altered within typical ranges for the Arctic. Also, drizzling cases are excluded from the model output.

Table 1. Description of Variables in Equation (6)

Variable	Description
$\log(\mathbf{LWC})_i$	$\log(\mathbf{LWC})$ at iteration step i
$\mathbf{y}$	Measurement vector consisting of ***dBZ*** and LWP
$\mathrm{F}(\log(\mathbf{LWC}))$	Forward model relating $\log(\mathbf{LWC})$ to the measurement (see equations (4) and (5))
$\mathbf{K}_i$	Jacobian matrix, or $\partial \mathrm{F}/\partial \log(\mathbf{LWC})_i$
$\mathbf{S}_\varepsilon$	Error covariance matrix of the measurement vector $\mathbf{y}$
$\overline{\log(\mathbf{LWC})}$	Mean profile of LWC, which is used as the a priori profile
$\mathbf{S}_{ap}$	Covariance matrix of the LWC profile

2.2.2. Error Covariances and A Priori Profile

[11] The two parameters *Z* and LWC are calculated from the model output DSDs, and a *dBZ*-log(LWC) relation is derived in the form of equation (4) using least squares minimization. The errors in retrieved *dBZ* due to this regression are interpreted as measurement errors and are, together with the actual noise errors of the radar measurement (1 *dBZ*; *Uttal and Kropfli* [2001]) included to form the error estimate ε_{dBZ}. Taking both errors into account ε_{dBZ} is determined to be 15.2 dBZ^2. Additionally, with the knowledge of the LWP retrieval error (ε_{LWP}), the measurement error covariance matrix has the following form

$$\mathbf{S}_\varepsilon = \begin{pmatrix} \varepsilon_{dBZ,1} & 0 & 0 & 0 & 0 \\ 0 & \varepsilon_{dBZ,2} & 0 & 0 & 0 \\ 0 & 0 & \dots & 0 & 0 \\ 0 & 0 & 0 & \varepsilon_{dBZ,ncld} & 0 \\ 0 & 0 & 0 & 0 & \varepsilon_{LWP} \end{pmatrix}, \quad (7)$$

and the indices 1 through *ncld* denote the height index within the cloud and *ncld* describing the number of cloudy levels. All errors are assumed to be Gaussian distributed and uncorrelated in height.

[12] An a priori profile of log(LWC) and the corresponding covariance matrix is also derived from the model output. To account for different vertical cloud extents, cloud statistics are derived based on their relative position within the cloud (PIC). First, for each modelled cloud with a vertical extent of 90 m (two levels) or more, log(LWC) values are calculated for the outer boundaries, i.e., cloud top level (*top*) and cloud bottom level (*bot*). Next, if a cloud has more than two levels, log(LWC) values are calculated for the inner next levels moving from cloud bottom to cloud center and from cloud top to cloud center. If the number of cloud levels is odd, a value is calculated for the cloud center level (*mid*).

Within this PIC system, the mean log(LWC) profile and its covariance matrix are written in the following form:

$$\overline{\log(\mathbf{LWC})} = \begin{pmatrix} \overline{\log(\mathrm{LWC})}_{bot} \\ \overline{\log(\mathrm{LWC})}_{bot+1} \\ \cdots \\ \overline{\log(\mathrm{LWC})}_{mid} \\ \cdots \\ \overline{\log(\mathrm{LWC})}_{top-1} \\ \overline{\log(\mathrm{LWC})}_{top} \end{pmatrix}, \quad (8)$$

and

$$\mathbf{S}_{ap} = \begin{pmatrix} c_{bot,bot} & c_{bot,bot+1} & \cdots & c_{bot,mid} & \cdots & c_{bot,top-1} & c_{bot,top} \\ c_{bot+1,bot} & c_{bot+1,bot+1} & \cdots & c_{bot+1,mid} & \cdots & c_{bot+1,top-1} & c_{bot+1,top} \\ \cdots & \cdots & \cdots & \cdots & \cdots & \cdots & \cdots \\ c_{mid,bot} & c_{mid,bot+1} & \cdots & c_{mid,mid} & \cdots & c_{mid,top-1} & c_{mid,top} \\ \cdots & \cdots & \cdots & \cdots & \cdots & \cdots & \cdots \\ c_{top-1,bot} & c_{top-1,bot+1} & \cdots & c_{top-1,mid} & \cdots & c_{top-1,top-1} & c_{top-1,top} \\ c_{top,bot} & c_{top,bot+1} & \cdots & c_{top,mid} & \cdots & c_{top,top-1} & c_{top,top} \end{pmatrix}, \quad (9)$$

with $\overline{\log(\mathbf{LWC})}_i$ ($i = bot, bot+1, \ldots, mid, \ldots, top-1, top$) denoting the mean log(LWC) at a specified PIC and $c_{i,j}$ the covariance between log(LWC) at PIC i and PIC j. As will be explained in section 3.1, *ncld* is set to 15 cloud levels in this study. Figure 1 shows that the frequency of occurrence at each PIC level decreases from the outer cloud boundaries towards the center of the cloud due to the fact that every detected cloud has at least two levels (i.e., *bot* and *top* levels), but only clouds with a vertical extent of at least 14 levels contribute to levels $bot + 6$ and $top - 6$. The number of cases at level *mid* is about half as large as at levels *bot* and *top* because clouds with an odd number of levels occur approximately in 50% of the cases.

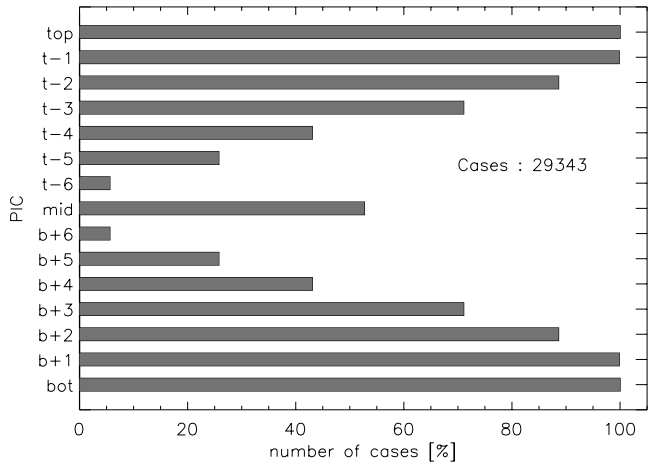

Figure 1. Occupancy of PIC levels in %. The values are 100% at cloud top (*top*) and cloud base (*bot*), because every cloud has a base and top, and decrease towards cloud interior due to the fact that clouds have different geometrical extents. The mid point of the cloud is only occupied if the number of cloud levels is odd.

3. Algorithm Comparison

3.1. Cloud Classification

[13] *Shupe et al.* [2001] developed a subjective cloud classification method that was used on a case-by-case basis for the SHEBA site. This classification attempts to distinguish between liquid, ice, mixed-phase, drizzling, raining, and snowing cloud events using the first three moments of the Doppler radar return together with LWP data from a dual-channel microwave radiometer, lidar depolarization ratios, and radiosonde data. This method is used to determine the liquid water cases to which both algorithms are applicable. Only single layer all-liquid cloud cases with no drizzle and no mixed-phase layer above are chosen from the time period of April to August 1998. Layers that are classified as pure ice are allowed to exist above the liquid clouds as the channels of the microwave radiometer are not sensitive to ice. Additionally, only clouds up to a maximum thickness of 675 m are included, corresponding to a maximum of 15 radar range gates. This is due to the fact that cloud occurrence statistics in reality and in the LES model are only similar for such clouds. Clouds thicker than 675 m occurred more often in the model output (∼40%) than in reality (∼20%), which means that these model clouds do not represent reality in an adequate way.

3.2. Algorithm Comparison Using SHEBA Data

[14] The L01 and F98 algorithms are applied to 9778 observations of single layer all-liquid, nondrizzling clouds on 45 different days from April to September 1998, corresponding to a total measurement time of 163 h. All of these clouds were measured simultaneously by cloud radar and microwave radiometer. An example comparison case (May 16, 1998) is shown in Figure 2, where two time periods are classified for application of the retrieval algorithms. In the following ε_{LWP} is calculated assuming a relative LWP-error of 30%. This case shows typical ranges of Arctic LWP, which only seldom exceed 150 g m^{-2}. The time span from 5 to 12 UTC is classified as drizzle. Generally, liquid water droplets within clouds with radii ranging from ∼20 to 400 μm are considered drizzle. From 0 to 4 UTC and 12 to 15 UTC, only minor differences between L01 and F98 results can been seen at first glance. The microwave-radiometer-derived LWP, which F98 is forced to conserve, corresponds quite closely to the LWP resulting from vertical integration of the L01 LWC profile. However, from 4 to 5 UTC, large differences in LWP of up to 100 g m^{-2} and more appear. The differences during this

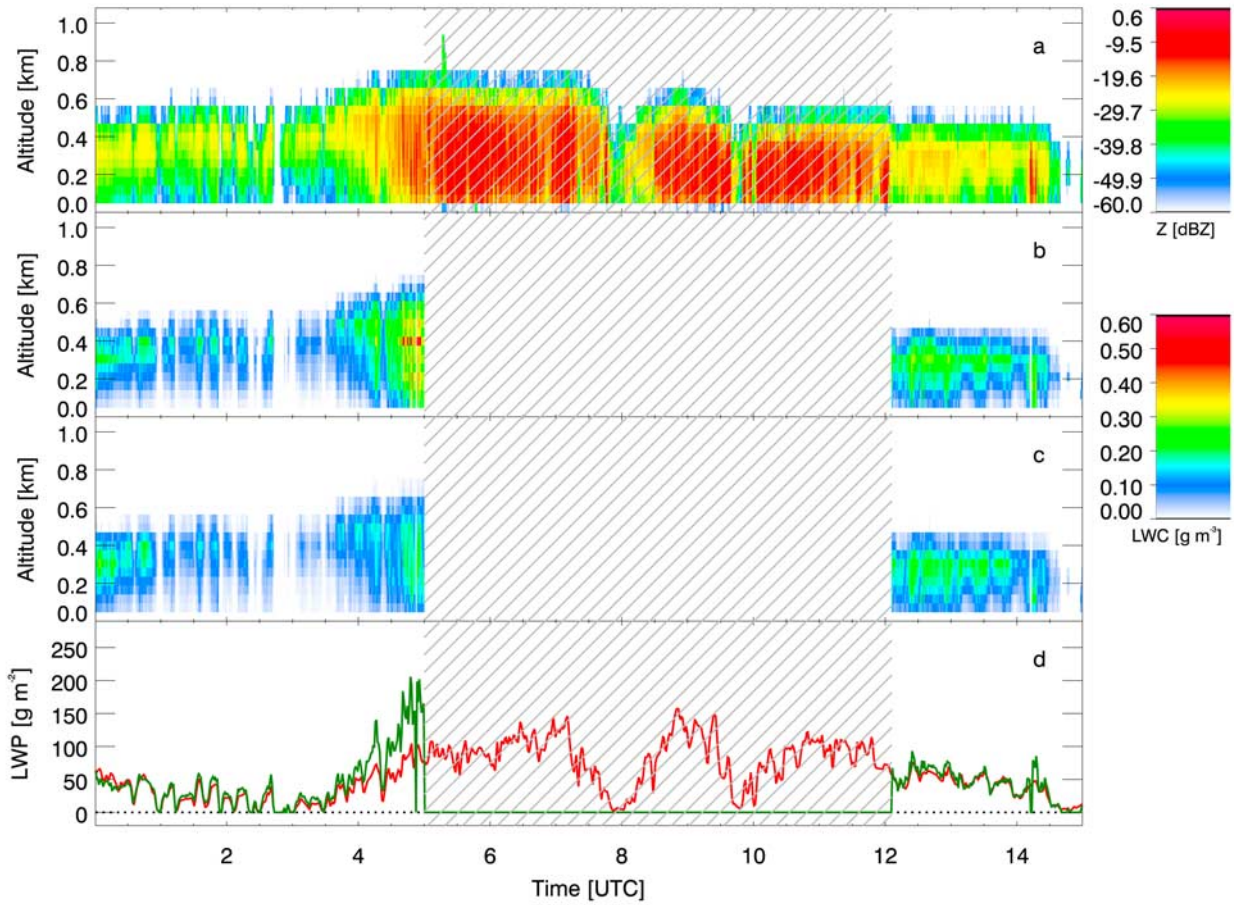

Figure 2. An example of Arctic, all-liquid stratus cloud to which the L01 and F98 methods were applied. (a) Time series of the *dBZ* profile; (b) and (c) time series of LWC profiles derived from L01 and F98, respectively, and (d) the microwave radiometer derived LWP (red) and the LWP resulting from L01 (green). The gray-shaded area shows the times when drizzle was present and thus the algorithms were not applicable.

time period are probably due to the onset of drizzle drops, which significantly increase Z and lead to an overestimation of LWC in the L01 retrieval.

[15] In the following analysis the L01 and F98 methods are applied to all cases during the specified time periods of study. Differences between F98 and L01 are shown in Figure 3 where ε_{LWP} is varied within the L01 method and F98 is left unchanged. The differences between L01 and F98 with ε_{LWP} calculated assuming a relative LWP error of 30% are shown in Figure 3a. In the middle of the cloud L01 produces larger LWC values than F98. This difference may be caused by larger drizzle droplets that lead to an overestimation in LWC. Another possible explanation may be that a larger number of cases have DSDs with larger drops, not necessarily drizzle drops, than in the LES model. Since the LES model is used to derive the *dBZ*-log(LWC) relation, this may explain the LWC overestimation.

[16] By calculating ε_{LWP} with a 30% LWP error, the LWP is a rather weak constraint on L01 and thus the characteristics of the *dBZ*-log(LWC) relation dominate the retrieval. In Figure 3b ε_{LWP} is determined with the LWP error set to 10%, which more strongly forces the L01-derived LWC profile to the LWP derived with the microwave radiometer. This is a fairer comparison when analyzing systematic differences between the two algorithms, because the F98-derived LWC profile is totally constrained to the derived LWP. This is, however, an unrealistic approach, because LWP cannot be measured to an accuracy of 10% using only two microwave channels (see section 5). With the 10% LWP error constraint the LWC bias between both techniques in the center of cloud has been reduced because the absolute values of L01 are now less dependent on Z. Also, the root-mean-square (rms) differences are reduced significantly. The number of cases was reduced to 8902 because the L01 algorithm did not converge for some cases due to the more restrictive LWP constraint. In the lower parts of the cloud F98 tends to retrieve higher LWC. To evaluate these differences further, the LES model output was used as an algorithm test bed.

3.3. Algorithm Comparison Using LES Model Output

[17] The advantage of using LES model output to evaluate the retrieval methods is that the retrieved LWC profiles can be evaluated against the model LWC profiles. To account for realistic measurement conditions a Gaussian error of 30% was added to the model LWP. However, bias

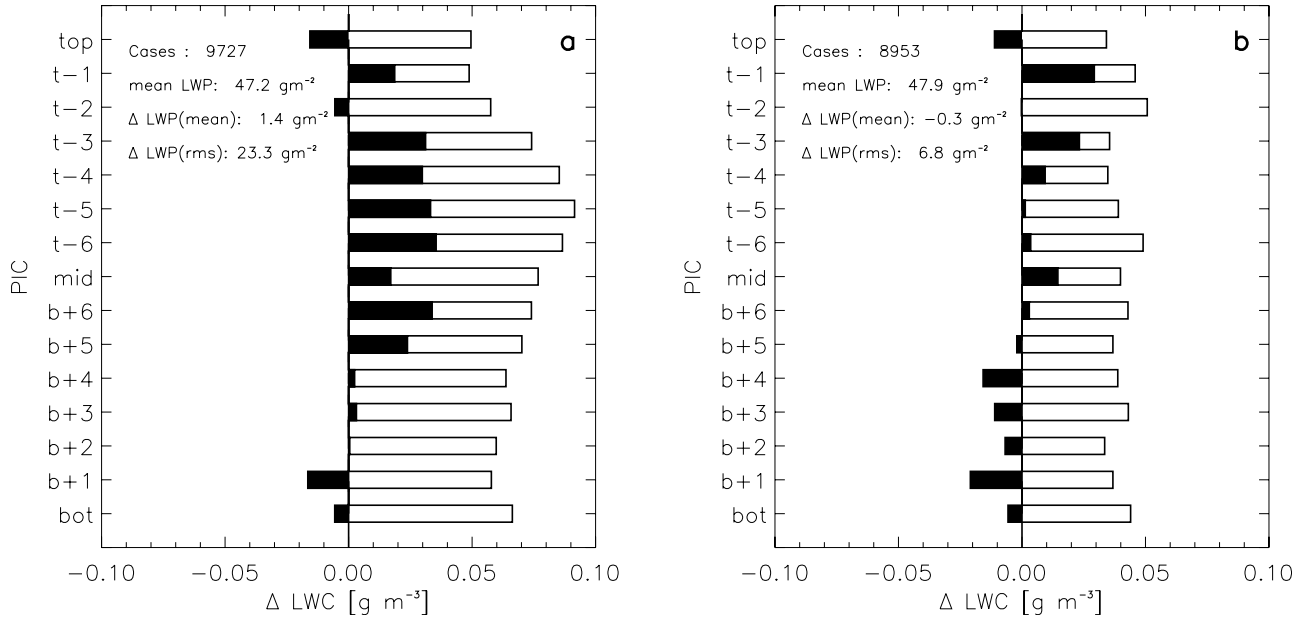

Figure 3. Mean (L01 - F98; black bars) and rms (white bars) difference as a function of position in cloud (PIC) when both methods are applied to the SHEBA data set. Theoretical LWP accuracies are set to either (a) 30% or (b) 10% in the L01 retrieval.

errors can dominate the LWP error due to uncertainty in the microwave gas absorption model and ambiguity due to a, strictly seen, underdetermined problem. The latter point addresses the fact, that different atmospheric situations (i.e., LWC, temperature, and humidity profiles) may give rise to the same brightness temperature combination. Such bias errors may vary on a daily basis [*Crewell and Löhnert*, 2003] and are thus, together with the absorption model uncertainty, interpreted as a random error. This is of need, since treating bias errors on a case-by-case basis is extremely difficult, as bias errors must be well known, which is mostly not the case. Accordingly, within L01, ε_{LWP} is determined using a 30% LWP accuracy. Also, according to section 2.2, a Gaussian error of 1 *dBZ* is added to the simulated *dBZ* measurements.

[18] One would expect the L01 method to perform more accurately, since the coefficients for the *Z*-LWC data set and the a priori information are derived from exactly this

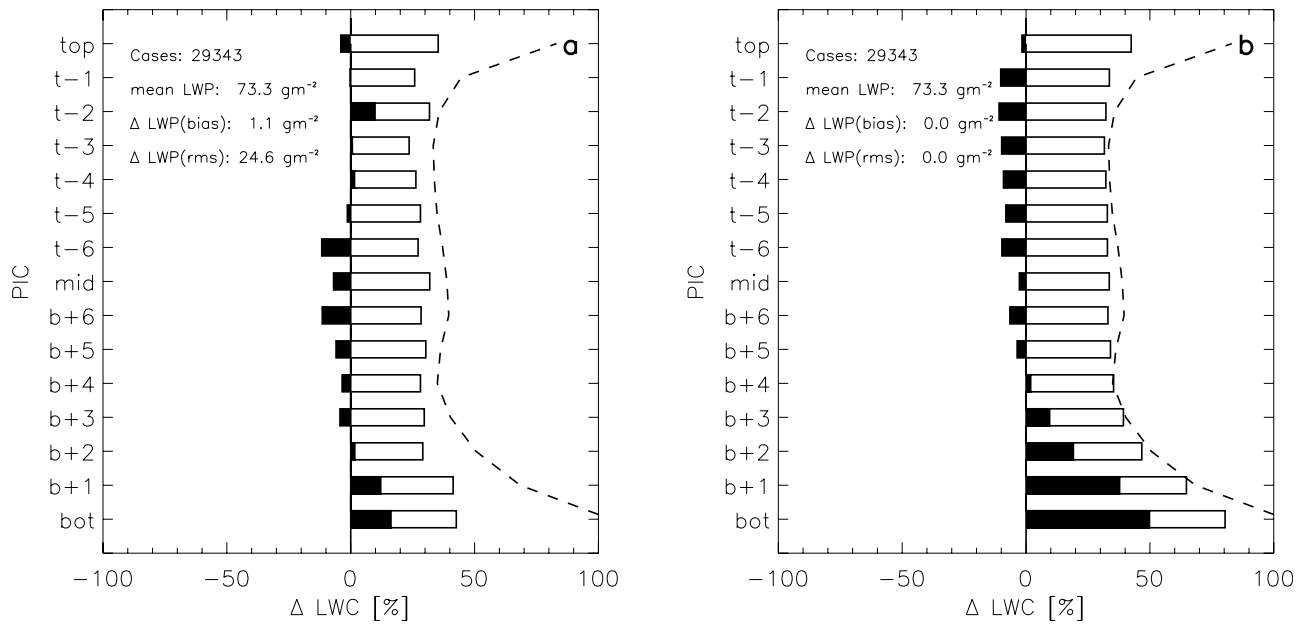

Figure 4. Bias (retrieval - model truth; black bars) and rms (white bars) errors as a function of PIC. (a) L01 - model truth, (b) F98 - model truth. Gaussian noise of 30% is applied to the model LWP values. Correspondingly, in L01 ε_{LWP} is set to 30%. The dashed line depicts the model LWC standard deviation at each PIC level. Errors are normalized by the LWC means of the model truth at each level.

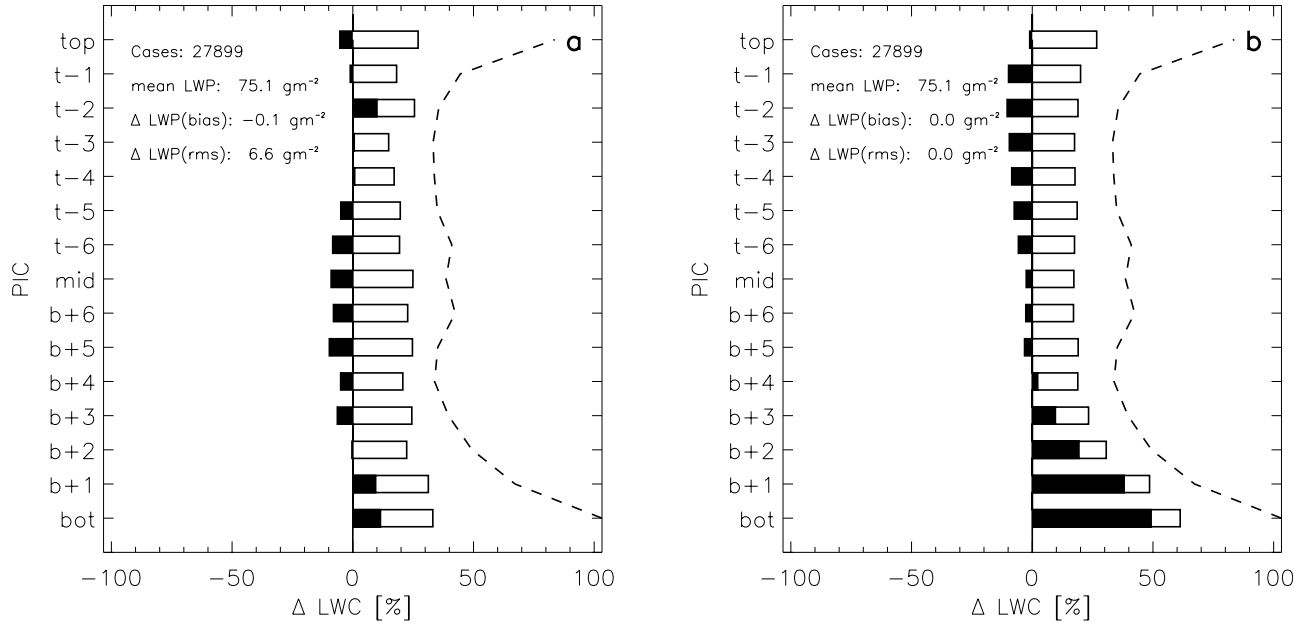

Figure 5. Bias (retrieval - model truth; black bars) and rms (white bars) errors as a function of PIC. (a) L01 - model truth, (b) F98 - model truth. Gaussian noise of 10% is applied to the model LWP values. Correspondingly, in L01 ε_{LWP} is set to 10%. The dashed line depicts the model LWC standard deviation at each PIC level. Errors are normalized by the LWC means of the model truth at each level.

model output. This behavior can be seen in Figures 4a and 4b, which show that the L01 LWC profiles, when compared to the F98 LWC profiles, have up to 30% smaller rms errors in the lower part of the cloud and ∼5% smaller rms errors in the upper part of the cloud. Also shown in Figure 4, as well as in Figures 5, 6, and 7, are the profiles of LWC standard deviation, which describes the variability of the model LWC with respect to the mean LWC profile. If the retrieval rms errors are larger than the standard deviation, the mean LWC profile contains more information about the actual LWC than the algorithm. It can be seen that the F98 method overestimates LWC by up to 50% in the lower part of the cloud. Similar behavior was shown by *Feingold et al.* [1994] when applying F98 to LES model output. We examine this behavior with sensitivity studies in section 4.

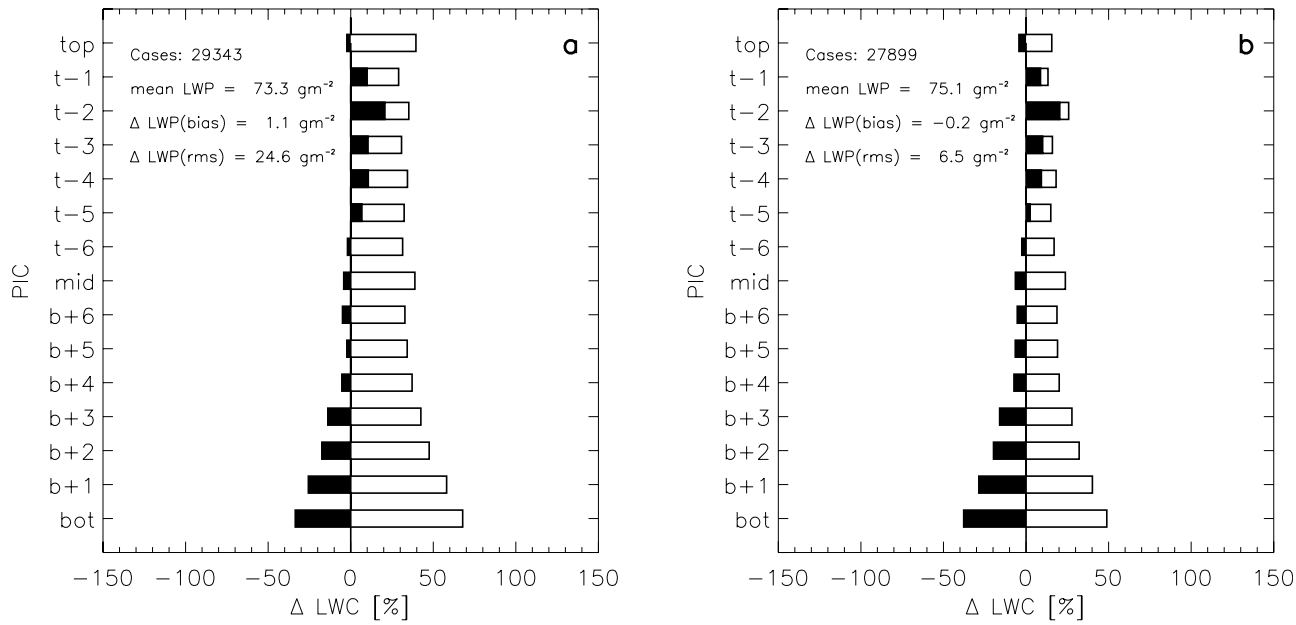

Figure 6. Bias (L01 - F98; black bars) and rms (white bars) differences as a function of position in cloud (PIC) when both methods are applied to the LES model output. Theoretical LWP accuracies are set to either (a) 30% or (b) 10% in the L01 retrieval.

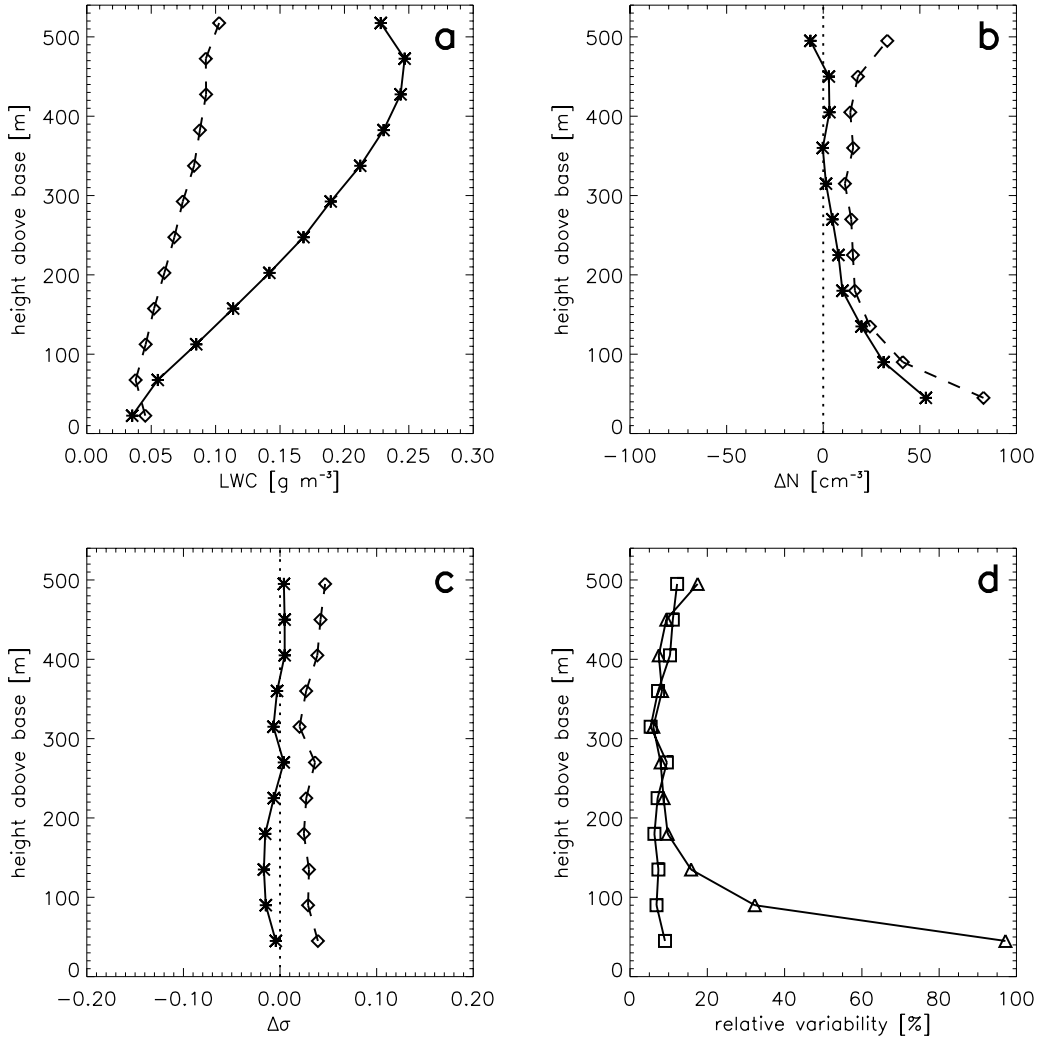

Figure 7. (a) The mean LWC profile (stars) and its standard deviation (diamonds) calculated from 2886 model clouds with vertical extents of 600 m, (b) mean differences (upper minus lower level, stars) and variabilities (mean quadratic difference, diamonds) of cloud droplet concentration N between two adjacent cloud levels, (c) mean differences (upper minus lower level, stars) and variabilities (diamonds) of cloud droplet distribution breadth σ between two adjacent cloud levels, and (d) relative variability (weighted with means) of N (triangles) and σ (squares).

[19] The impact of LWP accuracy is shown in Figure 5, where the model LWP is foreseen with a Gaussian noise of 10%. Correspondingly, within L01 ε_{LWP} is determined using a 10% LWP accuracy. The bias characteristics of both methods are similar to those in Figure 4, however the rms errors improve significantly (up to 20%) with respect to the LWC standard deviation. This result demonstrates the need to determine LWP with an accuracy of better than 30%.

[20] The results from using the LES model as a test bed can be compared to Figure 3. In Figures 6a and 6b the F98-derived LWC values are subtracted from the L01-derived values and are shown as relative bias and relative rms differences using a 30% ε_{LWP} and a 10% ε_{LWP}, respectively. In both cases, in the upper and middle parts of the cloud the rms differences are in the ranges of 30–40% and 20–30%, respectively, with biases less than 20%. In the lower parts of the cloud bias errors, mainly caused by F98 overestimation of LWC, dominate the errors. Comparing Figure 3 with Figure 6, the same tendency, i.e., F98 larger than L01 in the lower part of the cloud, can be observed. However, it is not possible to determine if the differences in Figure 3 are due to the same cause as in Figure 6, since "true" measurements of LWC are not available.

4. Assumptions Made by F98

[21] The two primary assumptions made in F98 are that drop number concentration and drop distribution breadth are independent of height. Measurements by *Slingo et al.* [1982] showed fairly constant values of N with height within marine stratocumulus. However, a database of in-situ measured low-level continental clouds was created by *Miles et al.* [2000], which shows high variations of N with height. Both F98-assumptions are tested using the LES LWC output for all model clouds with a geometrical depth

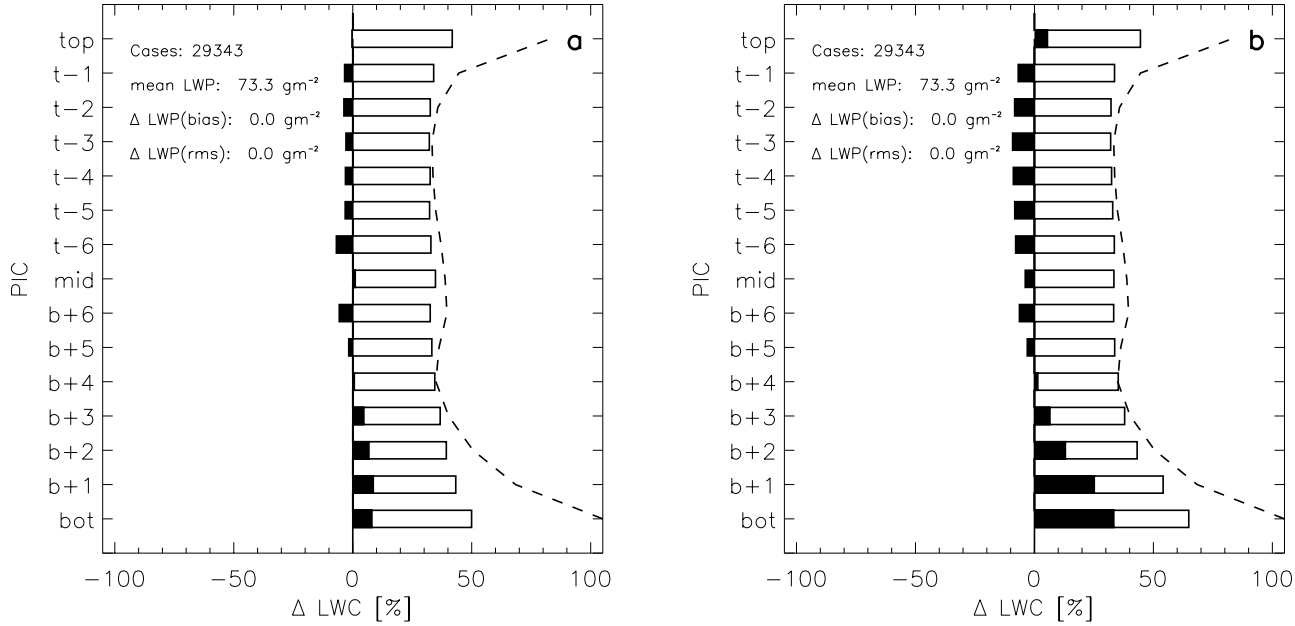

Figure 8. Bias (F98 - model truth; black bars) and rms (white bars) errors and their dependence on PIC. (a) F98 - model truth with height dependent N incorporated in F98, (b) F98 - model truth with height dependent σ incorporated in F98. A Gaussian noise of 30% was applied to the model LWP values. The dashed line depicts the LWC standard deviation at each PIC level. Errors are normalized by the LWC means of the model truth at each level.

of 14 levels (600 m) (Figure 7). The mean and standard deviation of the model LWC profiles are shown in Figure 7a, while Figures 7b and 7c show the mean differences and mean quadratic differences (variability) of N and σ between two adjacent cloud levels. The height dependent parameters σ and N are calculated from the model DSD. In the lower part of the cloud N increases rapidly with increasing height and the relative variability between two adjacent cloud levels is very high (15–100%) (Figure 7d). This means, that according to the model output, the assumption of constant N with height is not justified in the lower part of the cloud. In the upper half of the cloud the variability from level to level decreases to 10% with no significant mean increase or decrease. The logarithmic distribution breadth σ does not show a systematic increase or decrease from level to level (Figure 7c). The relative variability of σ between two cloud levels is low and constant at about 5–15% between all adjacent levels (Figure 7d). To investigate the influence of both assumptions, F98 was modified in the following two ways.

[22] If the assumption of constant N with height is not made while deriving equation (3) and only σ is assumed constant with height, the equation for LWC can be expressed as

$$\mathrm{LWC}_h = \frac{\mathrm{LWP}}{\Delta z_h} \cdot \frac{\sqrt{Z_h N_h}}{\sum_{j=1}^{M} \sqrt{Z_j N_j}}. \tag{10}$$

Assuming N to be given as a function of height, which of course is not the case in reality, we arrive at Figure 8a which shows the results of applying equation (10) to the LES model output and comparing with modelled LWCs. The bias in the upper and lower parts of the cloud has been diminished substantially in comparison to Figure 4b, showing that the assumption of constant N with height can result in systematic errors for clouds where N varies with height.

[23] If the assumption of height-constant σ is not made and only N is assumed constant with height, the equation for LWC can be expressed as

$$\mathrm{LWC}_h = \frac{\mathrm{LWP}}{\Delta z_h} \cdot \frac{\sqrt{Z_h}\exp\left(-9/2\sigma_h^2\right)}{\sum_{j=1}^{M} \sqrt{Z_j}\exp\left(-9/2\sigma_j^2\right)}. \tag{11}$$

Figure 8b shows the results when applying this equation to the LES model output. Both bias and rms error improve slightly in the lower part of the cloud. However, the overall bias behavior as seen in Figure 4b does not change substantially. The inclusion of a vertically resolved σ does not improve the LWC retrieval substantially because the assumption of a height-constant σ can be justified for the LES clouds which are examined. We therefore conclude that the F98 assumptions about N are the dominant factor leading to the bias characteristics seen here.

5. Conclusions

[24] This study has compared two algorithms for the retrieval of cloud LWC: the *Frisch et al.* [1998] method and the *Löhnert et al.* [2001] method. The methods were applied to measured data from the SHEBA campaign and

to a LES model used as a test bed for evaluating the algorithms.

[25] The retrieval of accurate cloud LWC profiles from the L01 and F98 methods is strongly dependent on accurate LWP retrievals from microwave radiometer measurements. Even a LWP error estimate of 30% is probably too low for low-LWP Arctic clouds. In cases of supercooled water clouds with small amounts of LWP, errors can be as high as a factor of 2 [*Doran et al.*, 2002]. An offset error in LWP will directly affect the F98 results in a way such that each LWC value will be offset in the same direction and by the same relative amount. The L01 method has the flexibility of directly incorporating the LWP error in the retrieval as a weighted constraint, but the constraint may be so weak that the influence of the *dBZ*-log(LWC) relation may become too strong leading, e.g., to a LWC overestimation in the case of larger drops. To successfully apply these algorithms to low-LWP Arctic liquid clouds, LWP algorithms are required, which use more information than two microwave brightness temperatures, such as more microwave frequencies [*Crewell et al.*, 2001; *Solheim et al.*, 1998] or additional instrumentation (IR radiometer, ceilometer) [*Crewell and Löhnert*, 2003]. Errors also arise due to uncertainties in gas and liquid water absorption, especially at temperatures below 0°C [*Westwater et al.*, 2001; *Lin et al.*, 2001].

[26] Nevertheless, the sensitivity studies shown in this paper indicate systematic errors even if LWP is assumed to have an error close to zero. Applying the algorithms to the LES model output suggests that the F98 method overestimates LWC in the lower part of clouds. This systematic difference was shown to originate largely from the assumption of constant N with height made in the F98 method. Similar systematic differences between L01 and F98 appear in the lower part of the cloud when applying both methods to the measured SHEBA data and to the model output. This may indicate that, within the SHEBA data set, F98 also overestimates LWC in the lower part of the cloud.

[27] The overall rms differences between L01 and F98 within the model test bed are shown to be on the order of 30 to 60% if realistic LWP error characteristics are assumed. Both algorithms strongly depend on the reflectivity profile, which can cause large rms errors, since no universal relation between the sixth and third moments for different cloud DSDs exists. Currently, an algorithm is being developed, that incorporates multi-channel microwave (19 channels) data, ceilometer data, cloud radar data, radiosonde data and certain physical constraints to obtain LWC profiles within an optimal estimation scheme. It is expected that such an approach will be more accurate, because the dependency of the new retrieval on Z will be reduced.

[28] If the L01 algorithm is to be applied to different climatic regions in future it should not be necessary to create a priori climatologies for each station. As the LWC climatology only poses a weak constraint to the algorithm, it will probably be sufficient to create four to five (e.g., Arctic, mid-latitude, sub-tropical, tropical) climatologies and to differentiate between a marine and a continental environment. To create such a database would require statistically representative radiosonde profiles for each climate and a one time, time intensive cloud model computing effort. Additionally to simulated LWC profiles, the database might also include airborne in-situ measurements from different locations. Further, to make the algorithm more physically consistent, one can use ancillary measurements of temperature and humidity to choose an a priori profile from the database. Together with information on cloud thickness, cloud base and cloud top an a priori profile may be chosen for each situation, which is physically more sensible than a simple mean LWC profile.

[29] **Acknowledgments.** This work was made possible by the German Academic Exchange Service ("DAAD Doktorandenstipendium im Rahmen des gemeinsamen Hochschulsonderprogramms III von Bund und Ländern") and was supported by the NASA FIRE/Arctic Clouds Experiment under agreement L14997. The material presented here is also based upon work supported by the National Science Foundation under grant 0084257. We further acknowledge the work of Hongli Jiang for her support concerning the LES model calculations.

References

Crewell, S., and U. Löhnert, Accuracy of cloud liquid water path from ground-based microwave radiometry, 2, Sensor accuracy and synergy, *Radio Sci.*, *38*(3), 8042, doi:10.1029/2002RS002634, 2003.

Crewell, S., H. Czekala, U. Löhnert, T. Rose, C. Simmer, R. Zimmermann, and R. Zimmermann, Microwave radiometer for cloud carthography: A 22-channel ground-based microwave radiometer for atmospheric research, *Radio Sci.*, *36*, 621–638, 2001.

Curry, J. A., et al., FIRE Arctic Clouds Experiment, *Bull. Am. Meteorol. Soc.*, *81*, 5–29, 2000.

Doran, J. C., S. Zhong, J. C. Liljegren, and C. Jakob, A comparison of cloud properties at a coastal and inland site at the North Slope of Alaska, *J. Geophys. Res.*, *107*(D11), 4120, doi:10.1029/2001JD000819, 2002.

Feingold, G., A. S. Frisch, B. Stevens, and W. R. Cotton, Radar/radiometer retrievals of cloud liquid water and drizzle: Analysis using data from a 3-D LES simulation of marine stratocumulus clouds, paper presented at DOE Science Team Meeting, Dep. of Energy, Charlotte, N. C., March 1994.

Fox, N., and A. J. Illingworth, The retrieval of stratocumulus cloud properties by groundZ-based cloud radar, *J. Appl. Meteorol.*, *36*, 485–492, 1997.

Frisch, A. S., C. W. Fairall, and J. B. Snider, Measurement of stratus clouds and drizzle parameters in ASTEX with a Ka-band Doppler radar and a microwave radiometer, *J. Atmos. Sci.*, *52*, 2788–2799, 1995.

Frisch, A. S., G. Feingold, C. W. Fairall, T. Uttal, and J. B. Snider, On cloud radar and microwave radiometer measurements of stratus cloud liquid water profiles, *J. Geophys. Res.*, *103*, 23,195–23,197, 1998.

Jiang, H., G. Feingold, W. R. Cotton, and P. G. Duynkerke, Large-eddy simulations of entrainment of cloud condensation nuclei into the Arctic boundary layer: May 18, 1998, FIRE/SHEBA case study, *J. Geophys. Res.*, *106*, 15,113–15,122, 2001.

Liao, L., and K. Sassen, Investigation of relationships between Ka-Band radar reflectivity and ice liquid water contents, *Atmos. Res.*, *34*, 231–248, 1994.

Lin, B., P. Minnis, A. Fan, J. A. Curry, and H. Gerber, Comparison of cloud liquid water paths derived from in situ and microwave radiometer data taken during the SHEBA/FIREACE, *Geophys. Res. Lett.*, *28*, 975–978, 2001.

Löhnert, U., S. Crewell, A. Macke, and C. Simmer, Profiling cloud liquid water by combining active and passive microwave measurements with cloud model statistics, *J. Atmos. Oceanic Technol.*, *18*, 1354–1366, 2001.

McFarlane, S. A., K. F. Evans, and A. S. Ackerman, A Bayesian algorithm for the retrieval of liquid water cloud properties from microwave radiometer and millimeter radar data, *J. Geophys. Res.*, *107*(D16), 4317, doi:10.1029/2001JD001011, 2002.

Miles, L. N., J. Verlinde, and E. E. Clothiaux, Cloud droplet size distributions in low-level stratiform clouds, *J. Atmos. Sci.*, *57*, 295–311, 2000.

Rodgers, C. D., *Inverse Methods for Atmospheric Sounding: Theory and Practice*, World Sci., River Edge, N. J., 2000.

Shupe, M. D., T. Uttal, S. Y. Matrosov, and A. S. Frisch, Cloud water contents and hydrometeor sizes during the FIRE Arctic clouds experiment, *Geophys. Res. Lett.*, *106*, 15,015–15,028, 2001.

Slingo, A. S., S. Nicholls, and J. Schmetz, Aircraft observations of marine stratocumulus during JASIN, *Q. J. R. Meteorol. Soc.*, *108*, 833–856, 1982.

Solheim, F., J. R. Godwin, E. R. Westwater, Y. Han, S. J. Keihm, K. Marsch, and R. Ware, Radiometric profiling of temperature, water

vapor and cloud liquid using various inversion methods, *Radio Sci.*, *33*, 393–404, 1998.

Ulaby, F. T., R. K. Moore, and A. D. Fung, *Microwave Remote Sensing Active and Passive*, vol. 1, 456 pp., Artech House, Norwood, Mass., 1981.

Uttal, T., and R. A. Kropfli, The effect of radar pulse length on cloud reflectivity statistics, *J. Atmos. Oceanic Technol.*, *18*, 947–961, 2001.

Uttal, T., et al., The surface and heat budget of the Arctic Ocean, *Bull. Am. Meteorol. Soc.*, *83*, 255–276, 2002.

Westwater, E. R., Y. Han, M. D. Shupe, and S. Y. Matrosov, Analysis of integrated cloud liquid and precipitable water vapor retrievals from microwave radiometers during SHEBA, *J. Geophys. Res.*, *106*, 32,019–32,030, 2001.

G. Feingold, M. D. Shupe, and T. Uttal, Environmental Technology Laboratory, NOAA, 325 Broadway, Boulder, CO 80303, USA. (graham.feingold@noaa.gov; matthew.shupe@noaa.gov; tuttal@etl.noaa.gov)

A. S. Frisch, Cooperative Institute for Research in the Atmosphere, 325 Broadway, Boulder, CO 80303, USA. (shelby.frisch@noaa.gov)

U. Löhnert, Meteorologisches Institut der Universität Bonn, Auf dem Hügel 20, 53121 Bonn, Germany. (uloeh@uni-bonn.de)